Ethyl Vinyl Acetate Copolymer—$SrAl_2O_4$:Eu,Dy and $Sr_4Al_{14}O_{25}$:Eu,Dy Phosphor-Based Composites: Preparation and Material Properties

S. B Mishra,[1,2] A. K. Mishra,[1,2,3] A. S. Luyt,[3] N. Revaprasadu,[4] K. T. Hillie,[1,5] W. J. vdM Steyn,[2,6] E. Coetsee,[1] H. C. Swart[1]

[1]*Department of Physics, University of the Free State, Bloemfontein 9300, Republic of South Africa*
[2]*CSIR Built Environment, CSIR, Pretoria 0001, Republic of South Africa*
[3]*Department of Chemistry, University of the Free State (Qwaqwa Campus), Private Bag X13, Phuthaditjhaba 9866, Republic of South Africa*
[4]*Department of Chemistry, University of Zululand, Private Bag X1001, KwaDlangezwa 3886, Republic of South Africa*
[5]*National Centre for Nano-Structured Materials, CSIR, Pretoria 0001, Republic of South Africa*
[6]*Department of Civil Engineering, University of Pretoria, Pretoria 0001, Republic of South Africa*

Received 31 March 2009; accepted 18 June 2009
DOI 10.1002/app.30976
Published online 8 September 2009 in Wiley InterScience (www.interscience.wiley.com).

ABSTRACT: New photoactive composite based on ethyl vinyl acetate (EVA) and $SrAl_2O_4$:Eu,Dy or $Sr_4Al_{14}O_{25}$:Eu,Dy were prepared by melt mixing or extrusion methodologies. The phosphorescent behavior and material properties of the polymer-phosphor composites were studied. The morphology of the polymer and the composites were studied by using scanning electron microscopy (SEM), transmission electron microscopy (TEM), and energy dispersive X-ray spectroscopy (EDS). The SEM shows that the physical and chemical behavior of the matrix and the extrusion conditions were primarily responsible for the surface morphology. TEM and EDS show that the phosphor particles were uniformly dispersed in the EVA matrix. A broad band of ultraviolet (UV)-excited phosphorescence of $SrAl_2O_4$:Eu,Dy and $Sr_4Al_{14}O_{25}$:Eu,Dy phosphors and the respective composites were observed at wavelengths of 516 nm and 490 nm, respectively. The photoluminescence (PL) spectra showed less intense phosphorescence but no shift in the wavelength of the emission peak for all the composites. The Hamburg wheel test was done on all the composites and the PL measurements before and after the test showed almost no change in the intensity of the emission. Thermal studies showed that the presence of the phosphors in the matrix slightly increased the crystallinity of EVA, which leads to higher melting enthalpies. Tensile testing shows very little change in the tensile strength and flexibility of the ethylene vinyl acetate copolymer. © 2009 Wiley Periodicals, Inc. J Appl Polym Sci 115: 579–587, 2010

Key words: ethylene vinyl acetate; $SrAl_2O_4$:Eu,Dy; composite; photoluminescence; phosphorescence

INTRODUCTION

Phosphorescence or afterglow can be defined as the delayed light emission from semiconductors or doped insulators at room temperature after the external excitation has stopped.[1] The afterglow is a luminescence with delayed radiative return that is caused by the trapping of photo-generated electrons and/or holes at intrinsic or extrinsic defect sites of the material. Thermal energy releases these trapped charge carriers that recombine at the ionized phosphorescent centers of the phosphors.[2–4] Eu^{2+} doped alkaline earth aluminate [MAl_2O_4:Eu^{2+}] phosphors (where M can be calcium, barium, or strontium) have been widely studied as these exhibit a rapid initial decay from Eu^{2+} ions with a long persistence. By codoping with other rare earth ions, an improvement in the intensity and the lifetime of the afterglow[5–7] can be obtained. The emission of Eu^{2+} depends on the host lattice and can occur from ultraviolet (UV) to the red region of the spectrum. This is due to the 5d → 4f transition and is associated with the change in electric dipole and the 5d excited state which is affected by the crystal field effect.[8,9]

$SrAl_2O_4$:Eu,Dy and $Sr_4Al_{14}O_{25}$:Eu,Dy phosphors possess safer, chemically stable, bright, and long-lasting photoluminescence (PL) compared with the conventional sulfide-based phosphors.[10–12] Strontium aluminate doped with Eu showed phosphorescence in the blue to green wavelength range. Codoping of this phosphor with rare earth ions such as Dy or Nd ions or including tens of mole percent more of Al_2O_3 than the stoichiometry prolongs the phosphorescence.[13–15] Because of these properties, these phosphors have a wide variety of applications, including luminous paints in highways, airports, buildings, ceramic products, textiles, outdoor night time displays, luminous clocks, and safety warnings.[16–22]

Correspondence to: H. C. Swart (swarthc.sci@ufs.ac.za).
Contract grant sponsors: National Research Foundation (NRF) of South Africa and the Council for Scientific, Industrial Research (CSIR) of South Africa.

To achieve excellent mechanical properties, optical transparency, shock and impact resistance, low-temperature processing ability and thermal stability, it is desirable to incorporate phosphors into various polymer matrices. Difficulties include poor water resistance,[23] serious emission concentration quenching, and very poor solubility of phosphors in the polymer matrix.[24] These areas are receiving attention internationally to improve the capacities of phosphors by developing composite materials using different methods.[25–29] Previous tests were done on the phosphorescent behavior and material properties of low-density polyethylene (LDPE) (MFI 7 g/10 min, density 0.918 g/cm^{-3}, 106°C), linear low-density polyethylene (LLDPE) (MFI 1 g/10 min, density 0.924 g/cm^{-3}, melting point 124°C), high-density polyethylene (HDPE) (density 0.95 g/cm^{-3}, melting point 130°C), and polypropylene (PP) (MFI 12 g/10 min, density 0.9 g/cm^{-3}, melting point 160°C), supplied by Sasol polymers.[30] The phosphorescence intensities of the polymer-phosphor composites were found to be lower than that of the pure phosphors. One of the probable reasons could be attributed to the fact of transparency and stability of the polymer matrices for UV radiations. LLDPE is known to have the best resistance for UV light and thus the matrix would not allow enough radiation to penetrate through the bulk to excite the phosphors and is seen as the main reason behind the poor emission of LLDPE. The duration of luminosity was reduced after the Hamburg wheel test for the various polymer-phosphor composites.

The objective of this study is to develop a material for illuminating road pavements at night. Ethyl vinyl acetate (EVA) was used as the matrix system due to its good clarity and gloss, which is required (as the primary requirement) for phosphorescence. It also possesses barrier properties, low-temperature toughness, stress crack resistance, hot melt adhesive, heat sealing properties, and stability to UV radiation.[31–33] EVA has a wide variety of applications such as cable insulating material, food packaging, thermoplastic elastomers, rubber, and drug delivery devices.[33–35]

In this study, EVA-$SrAl_2O_4$:Eu,Dy and $Sr_4Al_{14}O_{25}$:Eu,Dy phosphor-based composites were prepared using melt mixing and an extrusion method. The water absorption, the thermal and mechanical properties, as well as the composites' morphology were investigated. The Hamburg test (a standard road pavement test) was used to evaluate the resistance of the polymers to traffic load.

EXPERIMENTAL

Materials

EVA with 9% vinyl acetate (VA) content was supplied by Plastamid, Elsies River, South Africa. The melting point of the EVA is 95°C, and the density is 0.930 g cm^{-3}. Commercially available $SrAl_2O_4$:Eu,Dy and $Sr_4Al_{14}O_{25}$:Eu,Dy were obtained from Phosphor Technology (UK).

Preparation of nanocomposites

The EVA and phosphors were dried in an oven at 80°C overnight. These were melt blended using a Brabender mixer followed by extrusion. The phosphors (3% by weight) were mixed with EVA for 30 min at 130°C at a screw speed of 60 rpm. The samples were then extruded at an extrusion speed of 60 rpm at 130°C to obtain films with an average thickness of 0.45 ± 0.05 mm and an average width of 15 ± 1 mm.

Scanning electron microscopy and energy dispersive X-ray spectroscopy

Scanning electron microscopy (SEM) analyses of the nanocomposites were performed using a JEOL WIN-SEM-6400 electron microscope. The probe size was 115 nm, the probe current was 0.02 nA, and the

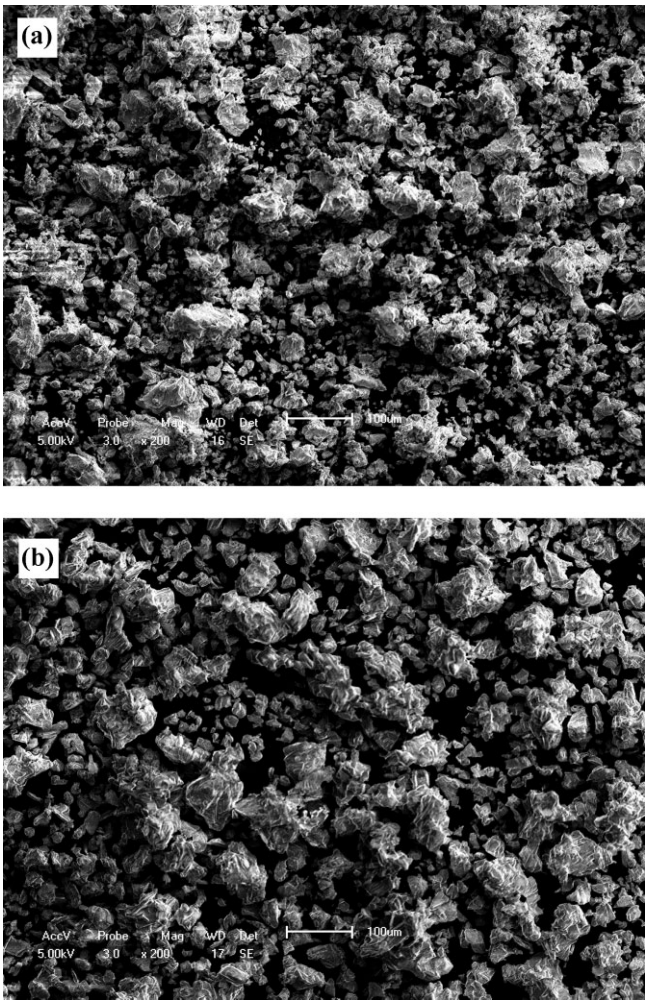

Figure 1 (a) SEM image of the $SrAl_2O_4$:Eu,Dy phosphor powder. (b) SEM image of the $Sr_4Al_{14}O_{25}$:Eu,Dy phosphor powder.

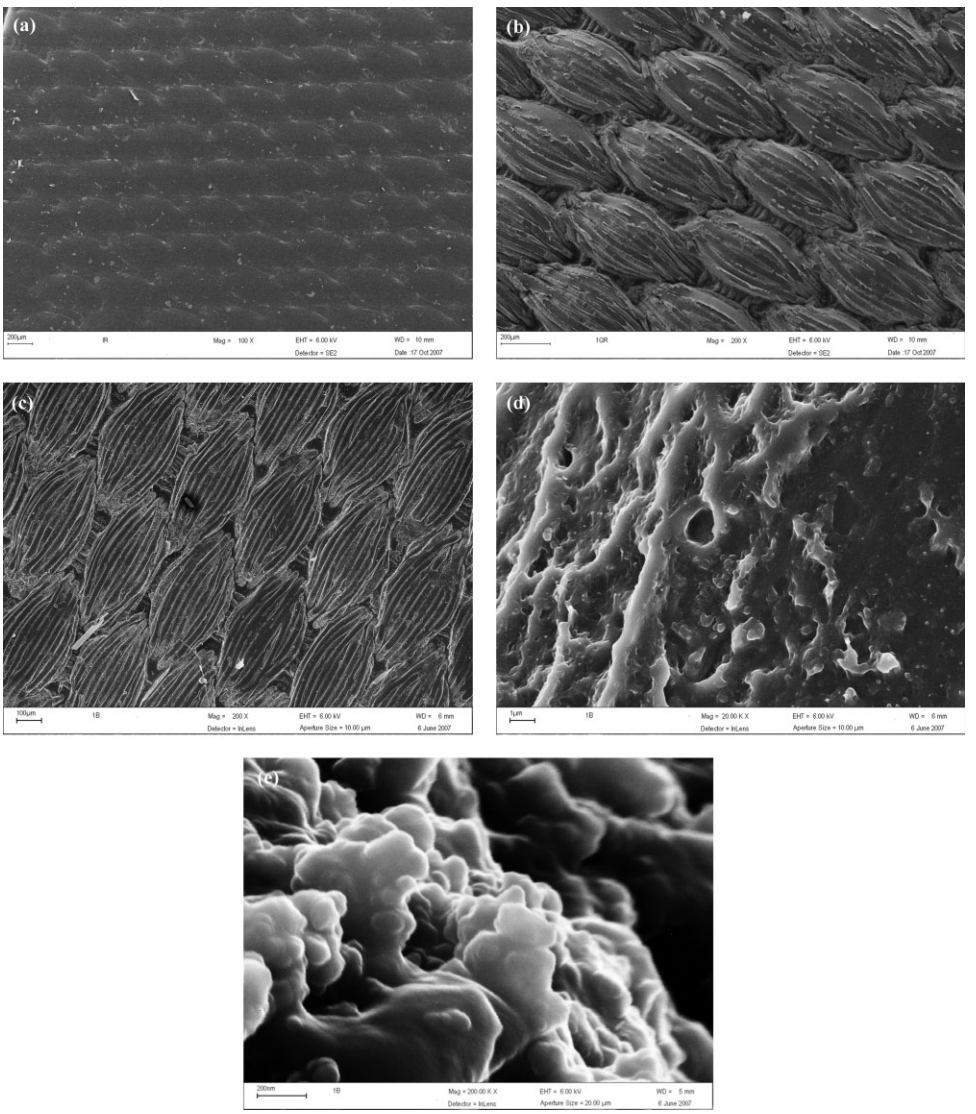

Figure 2 (a) SEM image of the surface of the EVA copolymer (×100). (b) SEM image of the surface of the EVA-SrAl$_2$O$_4$:Eu,Dy composite (×500). (c) SEM image of the surface of the EVA-$Sr_4Al_{14}O_{25}$:Eu,Dy composite (×200). (d) SEM image of the EVA-$Sr_4Al_{14}O_{25}$:Eu,Dy composite (×20,000). (e) SEM image of the EVA-$Sr_4Al_{14}O_{25}$:Eu,Dy composite(×200,000).

accelerating voltage was 5 keV. The surfaces of the samples were coated with gold to impart electrical conductivity. The energy dispersive X-ray spectroscopy (EDS) analyses were done using a Shimadzu SSX-550 SEM at an accelerating voltage of 15 kV and a working distance of 17 mm.

Transmission electron microscopy

The samples were prepared using cryo-ultramicrotomy. They were mounted on cryo-pins and frozen in liquid nitrogen. Sections were cut at −100°C using a Reichert FCS (Leica, Vienna, Austria) attached to a Reichert Ultracut S Ultramicrotome. The sections (100–150 nm thick) were collected on copper grids and viewed in a LEO 912 Omega (Carl Zeiss NTS GmbH, Oberkochen, Germany) transmission electron microscopy (TEM) operating at 120 kV.

Photoluminescence

The PL properties of the powdered phosphors SrAl$_2$O$_4$:Eu,Dy and $Sr_4Al_{14}O_{25}$:Eu,Dy and the thin films of composites with EVA were obtained using a Varian Cary Eclips Fluorescence spectrophotometer with a Xe flash lamp. Both excitation and emission spectra were obtained. The samples were excited at a wavelength of 320 nm to compare with other experiments that were done with a He-Cd laser ($\lambda =$ 325 nm). Special care was taken to make sure that experimental conditions were kept the same for all the samples.

Tensile testing

A Hounsfield H5KS universal testing machine was used to measure the tensile strength, tensile

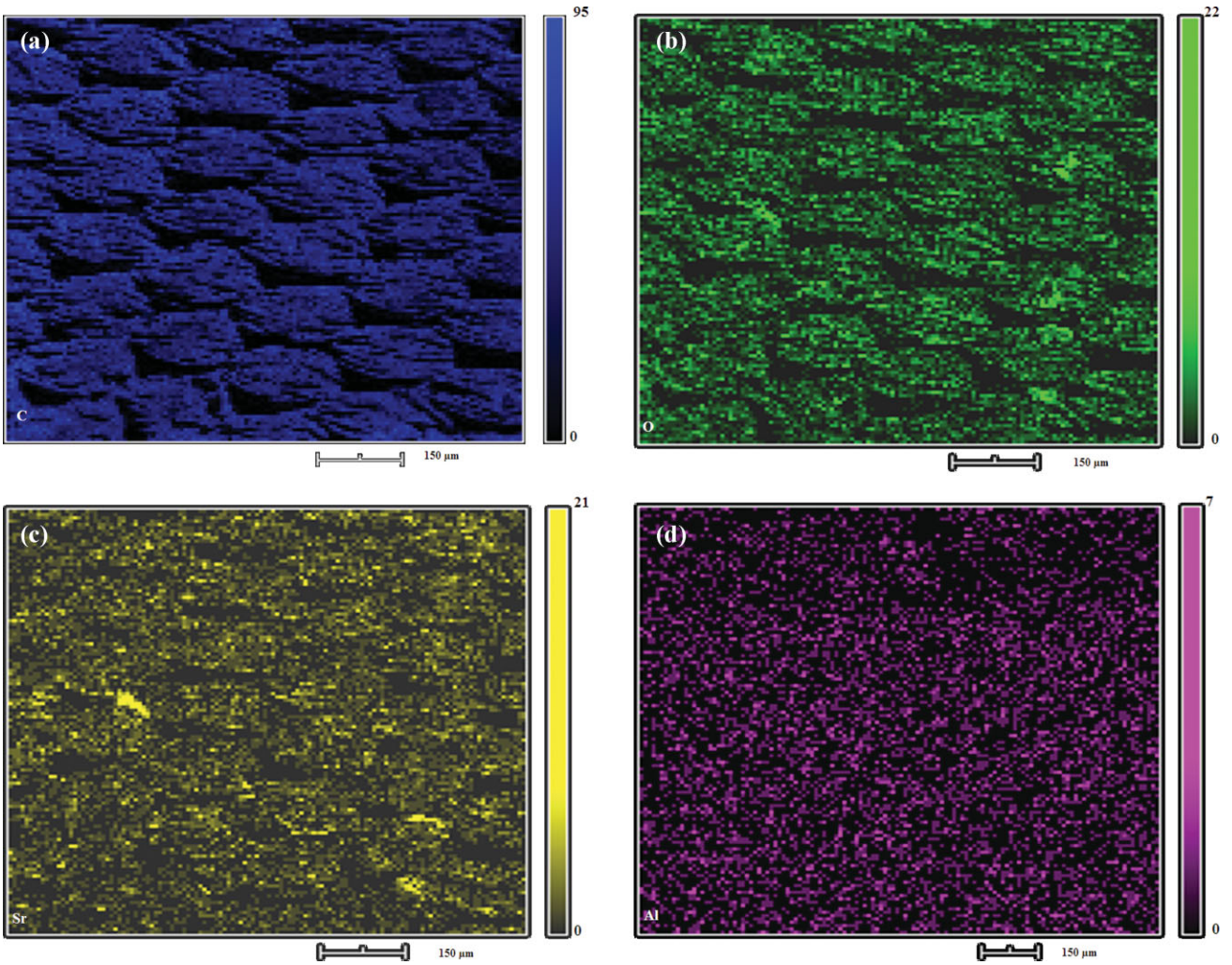

Figure 3 (a) SEM-EDX mapping of C in EVA-$Sr_4Al_{14}O_{25}$:Eu,Dy. (b) SEM-EDX mapping of O in EVA- $Sr_4Al_{14}O_{25}$:Eu,Dy. (c) SEM-EDX mapping of Sr in EVA- $Sr_4Al_{14}O_{25}$:Eu,Dy. (d) SEM-EDX mapping of Al in EVA- $Sr_4Al_{14}O_{25}$:Eu,Dy. [Color figure can be viewed in the online issue, which is available at www.interscience.wiley.com.]

modulus, and elongation properties of the nanocomposites. Samples of 150 mm × 15 mm × 0.45 mm were cut for tensile testing. Samples with a gauge length of 50 mm were tested at a crosshead speed of 50 mm min^{-1}. A continuous load-deflection curve was obtained. The averages and standard deviations of at least five tests per sample are reported.

Thermogravimetric analysis

Thermogravimetric analysis (TGA) was performed in a Perkin Elmer TGA7 thermogravimetric analyzer. The sample mass varied between 6 and 8 mg. The analyses were carried out from 30 to 600°C at a heating rate of 10°C min^{-1} under nitrogen atmosphere (flow rate 20 mL min^{-1}).

Differential scanning calorimetry

Differential scanning calorimetry (DSC) analyses were performed in a Perkin Elmer DSC7 DSC. The analyses were carried out on 5 to 10 mg samples between 30 to 200°C at a heating rate of 10°C min^{-1} under nitrogen atmosphere (flow rate 20 mL min^{-1}). The onset and peak temperatures of melting, as well as melting enthalpies, were obtained from the second heating cycle.

Water absorption

The samples were cut into 5 cm × 1 cm and weighed. This was followed by adding the samples in 200 mL of distilled water for 48 h. The samples surfaces were dried using filter paper at room temperature and water absorption was quantified as the percentage increase in weight[36]

$$W_m(\%) = \frac{W_f - W_i}{W_i} \times 100$$

Hamburg test

The Hamburg wheel test consists of a water bath in which asphalt slabs are embedded while being

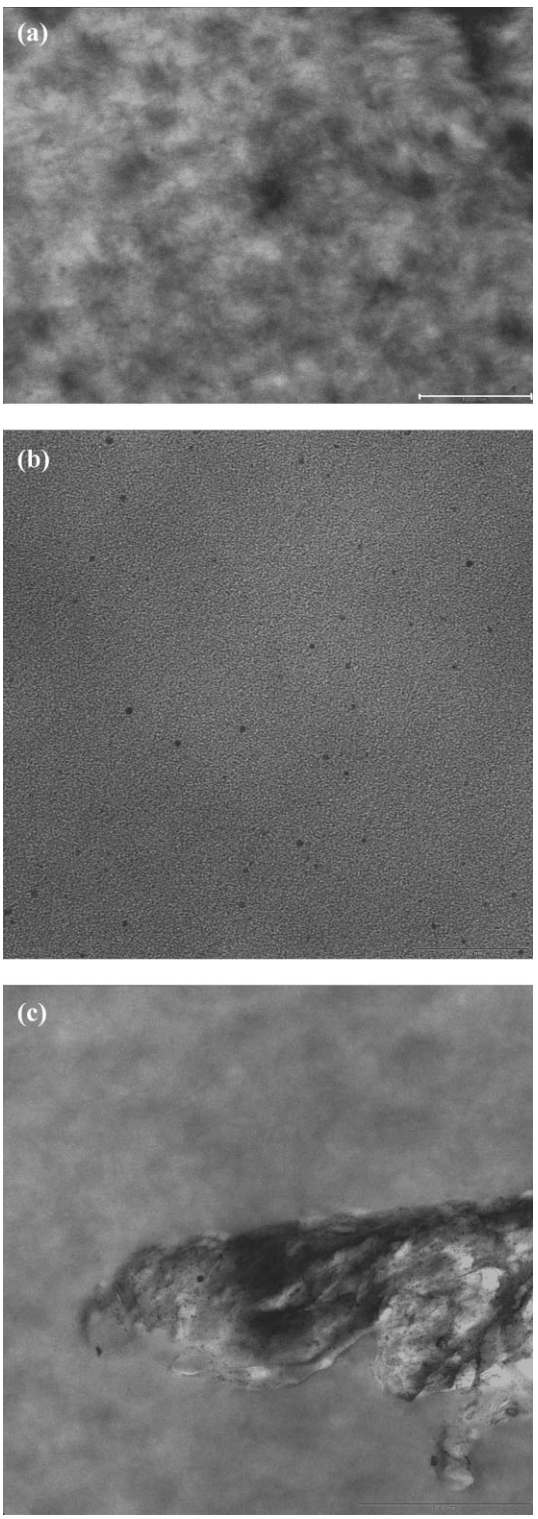

Figure 4 (a) TEM image of EVA copolymer. (b) TEM image of the rough surface of the EVA-$SrAl_2O_4$:Eu,Dy composite. (c) TEM image of the rough surface of the EVA-$Sr_4Al_{14}O_{25}$: Eu,Dy composite.

traversed with a test wheel exerting a load of 705 N onto the samples. In this application, composite samples of length of 5 cm, width of 1 cm, and thickness of 0.5 mm were attached to the surface of the asphalt slab while the slab was exposed to the action of the test wheel. This was done to measure the durability of the composite samples placed on the asphalt slabs against simulated traffic loads. The phosphorescence of the samples was measured before and after applying various loading regimes.

RESULTS AND DISCUSSION

Morphological studies

Figure 1(a,b) presents the SEM images of the pure $SrAl_2O_4$:Eu,Dy and $Sr_4Al_{14}O_{25}$:Eu,Dy phosphors,

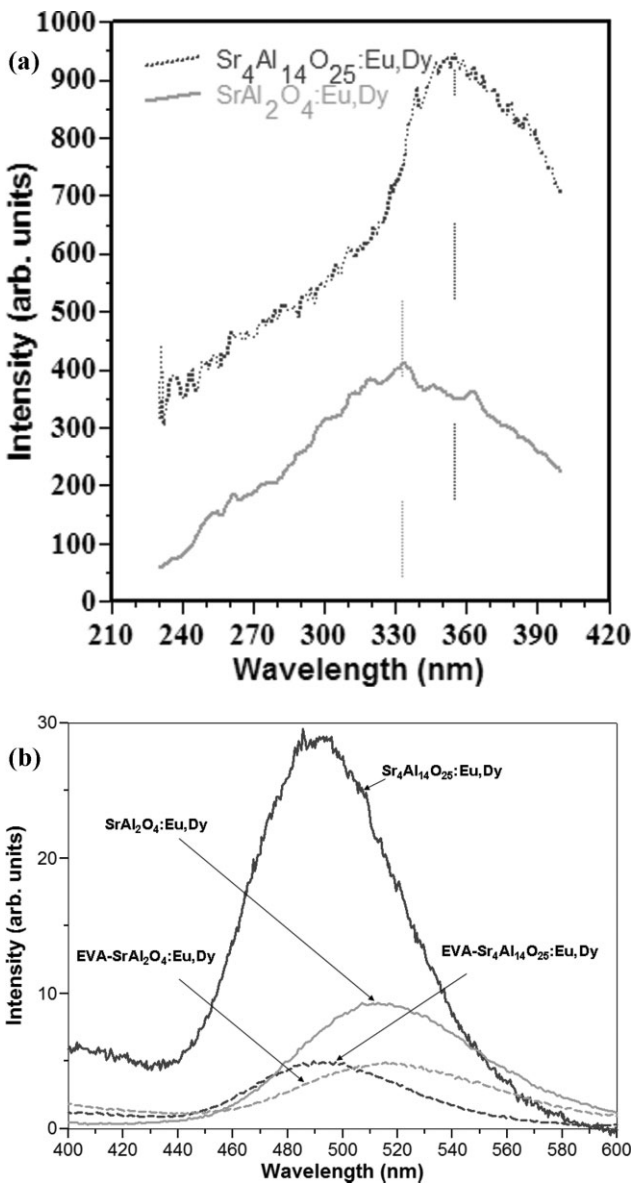

Figure 5 (a) PL excitation spectra of the $SrAl_2O_4$:Eu,Dy and $Sr_4Al_{14}O_{25}$:Eu,Dy pure phosphors. (b)PL emission spectra of the EVA-$SrAl_2O_4$:Eu,Dy and EVA-$Sr_4Al_{14}O_{25}$:Eu,Dy composites and pure phosphors.

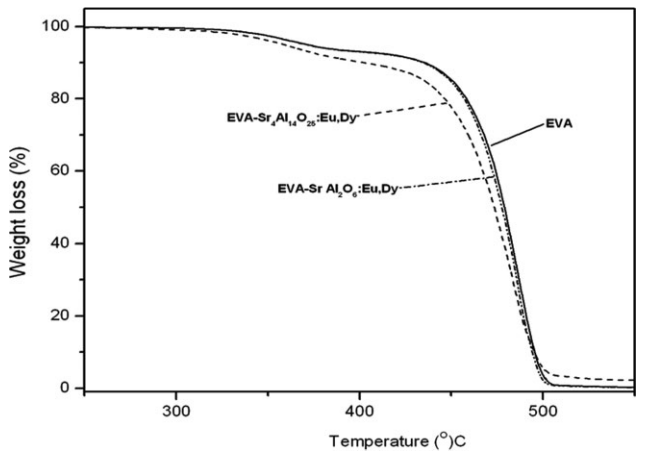

Figure 6 Thermo gravimetric analysis (TGA) curves of EVA, EVA-$SrAl_2O_4$:Eu,Dy and EVA-$Sr_4Al_{14}O_{25}$:Eu, Dy composites.

respectively. The images show irregular grains in the range of 8 to 80 μm. The SEM micrographs of polymer and polymer phosphor composites show a leaflet pattern, Figure 2(a–c). In the case of the polymer [Fig. 2(a)] the pattern was found to be a hollow leaflet, whereas in the case of the EVA-$SrAl_2O_4$:Eu,Dy [Fig. 2(b)] and $Sr_4Al_{14}O_{25}$:Eu,Dy [Fig. 2(c)] composites, the micrographs show tubular leaflet patterns. Dispersed phosphor particles and some large agglomerates in the matrix were also observed in the high-magnification images, namely Figures 2(d) and 1(e). The spherical particles can clearly be seen in the polymer matrix. From these various observations, it can be deduced that the formation of the leaflet pattern is probably the result of filler orientation in the direction of the shear force in the extruder, as well as the configuration of the extruder die on which the polymer/composite melt fell to form the thin strips.

Figure 3(a–d) shows the EDS mappings of the EVA-$Sr_4Al_{14}O_{25}$:Eu,Dy composite. Major elements detected were carbon, oxygen, strontium, and aluminum. Because of the low concentration of the doped rare earth elements, EDS could not detect any Eu or Dy. The mappings of the EVA-$Sr_4Al_{14}O_{25}$:Eu,Dy composite show that the carbon, oxygen, and strontium are evenly distributed in the leaflet pattern. The aluminum concentration was not high enough to clearly distinguish the leaflet structure on the aluminum scan.

The TEM images are shown in Figure 4(a–c). The images of the composites show the presence of the small phosphor particles in the matrix. The melt processing and extrusion allow the phosphor particles to uniformly disperse in the polymer matrix. No large agglomerates of phosphor particles were observed in the TEM micrographs. From the TEM micrographs, it can be deduced that good compatibility exists between the polymer matrix and the phosphors.

Photoluminescence studies

The excitation and emission spectra of $SrAl_2O_4$:Eu,Dy, $Sr_4Al_{14}O_{25}$:Eu,Dy and their EVA composites are shown in Figure 5(a,b). Broad excitation peaks with maxima at 333 and 353 nm were obtained for the $SrAl_2O_4$:Eu,Dy and $Sr_4Al_{14}O_{25}$:Eu,Dy phosphors, respectively as shown in Figure 5(a). The excitation ranges all fall within natural sunlight UV radiation, which made the phosphors excellent candidates to apply in infrastructure development. Bright green phosphorescence located at $\lambda = 0$ 520 nm could be observed for the $SrAl_2O_4$:Eu,Dy and the EVA-$SrAl_2O_4$:Eu,Dy composite after excitation with UV (320 nm) light, Figure 5(b). The $Sr_4Al_{14}O_{25}$:Eu,Dy and the EVA-$Sr_4Al_{14}O_{25}$:Eu,Dy composite phosphorescence were located at $\lambda = 495$ nm. All the emissions show a single peak with only one band, which is in agreement with earlier reports.[12] The crystal field at the sites of the phosphorescence ions and the degree of covalence (coordination number) of these ions with the surrounding O atoms are the two fundamental aspects that are responsible for determining the emission wavelength of the phosphor.[37,38] The crystal field allows splitting of the 5d level into sublevels. It is also reported that phosphorescence bands of the phosphor are quite sensitive to the refractive index of the polymer matrix. There is a linear relationship between the

TABLE I
DSC Results

	Second heating curve			Cooling curve		
Samples	Onset temperature (°C)	Peak temperature (°C)	Enthalpy (ΔH_m) (J g^{-1})	Onset temperature (°C)	Peak temperature (°C)	Enthalpy (ΔH_m) (J g^{-1})
EVA	81.6	94.2	36.1	85.6	79.5	−36.4
EVA-$Sr_4Al_{14}O_{25}$: Eu,Dy	87.7	96.7	41.5	84.9	79.8	−38.4
EVA-$SrAl_2O_4$: Eu,Dy	86.3	95.4	41.4	82.8	77.8	−41.5

TABLE II
Tensile Results

Samples	Elongation at yield (%)	Stress at yield (Mpa)	Elongation at break (%)	Stress at break (MPa)	E-modulus (MPa)
EVA	8.6 ± 0.8	5.9 ± 0.2	252.3 ± 44.5	6.8 ± 0.2	61.8 ± 0.8
EVA-$Sr_4Al_{14}O_{25}$:Eu,Dy	11.4 ± 3.6	5.8 ± 0.2	284.5 ± 53.2	6.9 ± 0.2	46.9 ± 14.7
EVA-$SrAl_2O_4$:Eu,Dy	11.2 ± 1.8	5.8 ± 0.1	312.5 ± 45.9	7.2 ± 0.4	56.4 ± 7.2

wavelength corresponding to the emission maximum and the refractive index term, namely n^2-$1/2n^2 + 1$.[28] In this study, the refractive index of the EVA matrix is constant for the two different phosphors in use. The presence of the polymer matrix in this case did not affect the wavelength but the intensity dropped, which was expected due to the attenuation of photons through the polymer matrix and the low concentration of the phosphor in the composite.

Thermal properties

Thermogravimetric studies

The thermogravimetric (TG) analyses were carried out in a nonoxidative environment under inert (N_2) gas flow to analyze the effect on the thermal degradation of the polymer in the presence of phosphorescent particles as filler. The TGA curve (Fig. 6) of the EVA and EVA-phosphor composites show two-step degradation. The onset temperature of the first step was in the range of 315 to 335 °C, which corresponds to the release of acetic acid and formation of C double bonds along the polymer backbone. At temperatures above 380°C, thermal degradation of the ethylene-co-acetylene main chain takes place. The degradation of EVA and EVA-$SrAl_2O_4$:Eu,Dy are similar, whereas early degradation of the EVA-$Sr_4Al_{14}O_{25}$:Eu,Dy composite is observed. The changes in the lattice of the phosphor and increased number of Sr defects probably play a key role in accelerating the thermal degradation of the composites.

DSC studies

Table I summarizes the onset and peak temperatures of melting and crystallization, as well as the melting and crystallization enthalpies, of pure EVA and the composites. The results are taken from the second heating and cooling cycles of the DSC analyses. The glass transition temperatures of all the three samples were in the order of -55 ± 1°C. The changes in the melting enthalpy values suggest that the crystallinity of the matrix is slightly influenced by incorporating the phosphor as a filler. The melting enthalpies of the composites were found to be somewhat higher than that of pure semicrystalline EVA which has a low crystallinity. This can be attributed to the fact that the phosphor particles act as nucleating sites for the formation of a higher number of crystallites due to intermolecular forces between the filler and matrix. Also, the intermolecular forces between polymer and phosphor aid the packing of composite into a three dimensional ordered structure restricting the chain mobility of EVA. This probably leads a rise in rigidity of the composites and an increase in the tensile strength can be presumed. There were no major differences between the melting peak temperatures of EVA and the EVA-phosphor composites. The crystallization results are in line with the melting results.

Mechanical properties

The mechanical properties of the EVA, EVA-$SrAl_2O_4$:Eu,Dy, and EVA-$Sr_4Al_{14}O_{25}$:Eu,Dy composites were evaluated through tensile testing (Table II). It has been reported that low-interfacial interaction between the embedding phosphors and the matrix results in poor mechanical properties. This low interaction leads to mechanical rupture at the polymer interface.[39] Although the DSC results indicated a slight increase in crystallinity for the two composites, the tensile results show only small differences between the tensile strength values of pure EVA and the two composites.

The elongation at break value and stress at break corresponding to the tensile strength for the polymer-phosphor composites seems to be higher than for the polymer itself. This therefore confirms that an increase in the total crystallinity as observed

TABLE III
Water Absorption Results

Samples	Initial weight [W_i (g)]	Final weight [W_f (g)]	Water absorption [W_m (%)]
EVA	0.2235	0.2236	0.044
EVA-$Sr_4Al_{14}O_{25}$:Eu,Dy	0.2548	0.2550	0.078
EVA-$SrAl_2O_4$:Eu,Dy	0.2339	0.2341	0.085

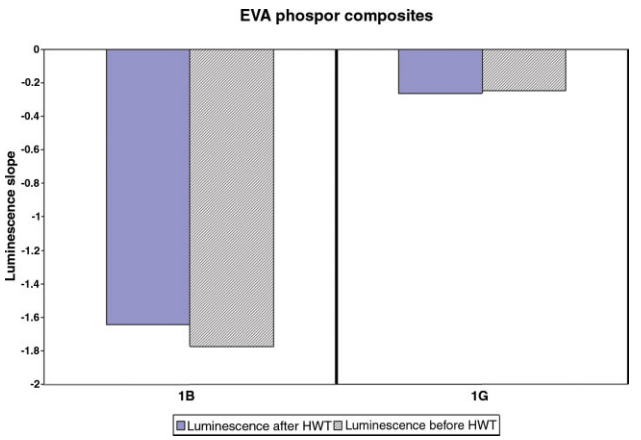

Figure 7 Photoluminescence slopes before and after the Hamburg test. [Color figure can be viewed in the online issue, which is available at www.interscience.wiley.com.]

during the thermal transition study influences the mechanical properties of the polymer-phosphor composite.

Water absorption studies

Coating with a water-resistant polymer matrix provides a barrier against water penetration through the matrix and reaction with the strontium aluminate. This provides an advantage for retaining the phosphorescence property which otherwise will be adversely affected.[23] Strontium aluminates are not resistant to water and react with it according to the reaction:

$$SrAl_2O_4 + 4H_2O \rightarrow Sr^{2+} + 8OH^- + 2Al^{+3}$$

Table III presents the water absorption results of the EVA and EVA-phosphor composites. The EVA absorbed a negligible amount (0.044%) of water, whereas the EVA-$Sr_4Al_{14}O_{25}$:Eu,Dy and EVA-$SrAl_2O_4$:Eu,Dy absorbed 0.078 and 0.085% of water, respectively. The increase in water absorption by the EVA-phosphor composites suggests that the polarity of the matrix and the phosphor promotes the hydrophilic behavior. This increase in the water absorption by the composite further strengthens the notion that polarity induces strong interfacial interactions between the matrix and the phosphor allowing the absorption of water.

Hamburg wheel tests

Hamburg tests were conducted to evaluate the durability of the polymers against simulated wheel loads and the effect of these wheel loads on the luminosity of the polymers. The data in Figure 7 show the decay curve (luminosity versus time) slopes of the two phosphor-polymer composites. A steep slope indicates a faster luminosity decay rate. The data indicate that the simulated wheel load of the Hamburg test did not have a profound effect on the polymers, with similar luminosity decay slopes before and after the application of simulated wheel loads.

CONCLUSIONS

EVA-phosphor composites were prepared using melt mixing and an extrusion technique. The wavelength of the emission by the phosphors was not influenced by incorporation in the composites, although the emission intensities were affected. The material properties such as thermal transition and increase in tensile strength suggest that the EVA-phosphor composites are slightly more crystalline. The phosphor enhances the hydrophilic behavior of the EVA. The afterglow of the EVA-phosphor composites remains unchanged even after the Hamburg wheel test. The phosphorescent property of the phosphor composites sustains even after the Hamburg wheel test.

We thank Prof. PWJ van Wyk from the Centre of Microscopy for the SEM and Mohamed Jaffer from University of Cape Town for the TEM measurements.

References

1. Claubau, F.; Rocquefelte, X.; Jobic, S., Deniard, P.; Whangbo, M. H.; Garcia, A.; Le Mercier, T. Chem Mater 2005, 17, 3904.
2. Clabau, F.; Rocquefelte, X.; Jobic, S.; Deniard, P.; Whangbo, M.-H.; Garcia, A.; Mercier, T. L. Solid State Sc 2007, 9, 608.
3. Shionoya, S.; Yen, W. Phosphor Handbook; CRC Press: New York, 1999.
4. Lin, Y.; Zhang, Z.; Zhang, F.; Tang, Z.; Chen, Q. Mater Chem Phys 2000, 65, 103.
5. Palilla, F. C.; Levine, A. K; Tomkus, M. R. J Electrochem Soc 1968, 115, 642.
6. Peng, T.; Yanga, H.; Pua, X.; Hua, B.; Jianga, Z.; Yan, C. Mater Lett 2004, 58, 352.
7. Lin, Y.; Tang, Z.; Zhang, Z.; Nan, C. J Eur Ceram Soc 2003, 23, 175.
8. Nag, A.; Kutty, T. R. N. J Alloys Comp 2003, 354, 221.
9. Blasse, G.; Grabmaier, B. C. Luminescent Materials; Springer: Berlin, 1994.
10. Jia, W. Y.; Yuan, H. B.; Yen, W. M. J Lumin 1998, 76, 424.
11. Groppi, G.; Cristiani, C.; Forzatti, P. J Mater Sci 1994, 29, 3441.
12. Peng, T.; Huajun, L.; Yang, H.; Yan, C. Mater Chem Phys 2004, 85, 68.
13. Nakazawa, E.; Murazaki, Y.; Saito, S. J Appl Phys 2006, 100, 113113.
14. Matsuzawa, T.; Aoki, Y.; Takeuchi, N.; Murayama, Y. J Electrochem Soc 1998, 143, 2670.
15. Ngaruiya, J. M.; Nieuwoudt, S.; Ntwaeaborwa, O. M.; Terblans, J. J.; Swart, H. C. Mater Lett 2008, 62, 3192.
16. Lu, Y.; Li, Y.; Xiong, Y.; Wang, D.; Yin, Q. Microelectronics J 2004, 35, 379.
17. Murayama, Y.; Takeuchi, N.; Aoki, Y.; Matsuzawa, T. U.S. Pat. 5,424,006 (1995).
18. Matsuzawa, T.; Aoki, Y.; Takeuchi, N.; Murayama, Y. J Electrochem Soc 1996, 143, 2670.

19. Katsumata, T.; Nabae, T.; Sasajima, K.; Kumuro, S.; Morikawa, T. J Electrochem Soc 1997, 144, L243.
20. Yamamoto, H.; Matsuzawa, T. J Lumin 1997, 72–74, 287.
21. Groppi, G.; Cristiani, C.; Forzatti, P. J Mater Sci 1994, 29, 3441.
22. Jia, W. Y.; Yuan, H. B.; Yen, W. M. J Lumin 1998, 76, 424.
23. Peng, L.; Luo, Y.; Dan, Y.; Zhang, L.; Xia, S.; Zhang, X. Colloid Polym Sci 2006, 285, 153.
24. Wang, D.; Zhang, J.; Lin, Q.; Fu, L.; Zhang, H.; Yang, B. J Mater Chem 2003, 13 2279.
25. Ueba, Y.; Banks, E.; Okamoto, Y. J Appl Polym Sci 1980, 25, 359.
26. Swada, T.; Ando, S. Chem Mater 1998, 10, 3368.
27. Kido, J.; Hayase, H.; Hongawa, K.; Okuyama, K. Appl Phys Lett 1994, 65, 2124.
28. Bhat, S. V.; Govindaraj, A.; Rao, C. N. R. Chem Phys Lett 2006, 422, 323.
29. Wang, H.; Lu, X.; Zhao, Y.; Wang, C. Mater Lett 2006, 60, 2480.
30. Mishra, S. B.; Mishra, A. K.; Revaprasadu, N.; Hillie, K. T.; Steyn, WJvdM.; Coetsee, E.; Swart, H. C. J Appl Poly Sci 2009, 112, 3347.
31. Zhu, J.; Morgan, A. B.; Lamelas, F. J.; Wilkie, C. A. Chem Mater 2001, 13, 74.
32. Marriot, W. R. Chen, E. Y.-X. J Am Chem Soc 2003, 125, 15726.
33. Garnweitner, G.; Smarsly, B.; Assink, R.; Ruland, W.; Bond, E.; Brinker, C. J.; J Am Chem Soc 2003, 125, 5626.
34. Alexandre, M.; Beyer, G.; Henrist, C.; Cloots, R.; Rulmont, A.; Jerome, R.; Dubois, P. Macromol Rapid Commun 2001, 22, 643.
35. Maiti, P.; Yamada, K.; Okamoto, M.; Ueda, K.; Okamoto K. Chem Mater 2002, 14, 4654.
36. Cypes, S. H.; Saltzman, W. M.; Giannelis, E. P. J Control Release 2003, 90, 163.
37. Bai, C. Y.; Zhang, X. Y.; Dai, J. B.; Zhang, C. Y. Prog Org Coat 2007, 59, 331.
38. Harnath, D.; Shanker, V.; Chander, H.; Sharma, P. J Phys D: Appl Phys 2003, 36, 2244.
39. Sun, J. Y.; Shi, C. S.; Li, Y. M.; Chin Sci Bull 1989, 34, 703.